Available online at www.sciencedirect.com
SCIENCE DIRECT
ELSEVIER
Journal of the European Ceramic Society 26 (2006) 1585–1590
ECERS
www.elsevier.com/locate/jeurceramsoc

Microstructure of nanoporous yttria-stabilized zirconia films fabricated by EB-PVD

Byung-Koog Jang *, Hideaki Matsubara

Materials Research and Development Laboratory, Japan Fine Ceramics Center (JFCC), 2-4-1 Mutsuno, Atsuta-ku, Nagoya 456-8587, Japan

Received 16 December 2004; received in revised form 14 March 2005; accepted 19 March 2005
Available online 23 May 2005

Abstract

Microstructures of ZrO_2–4 mol% Y_2O_3 coating layers fabricated by EB-PVD are characterized. Coating layers are found to consist of porous columnar grains with a feather-like structure containing evenly dispersed nano-sized gaps. Nanopores less than 50 nm in diameter could also be observed within columnar grains. The columnar grain size and column width of the coating layers increased with increasing coating thickness and substrate rotation speed. The porosity of the coating layers also shows increases with increasing substrate rotation speed. Specimens rotated at 1 rpm are found to contain wavy or scalloped columnar grains. Specimens rotated at higher speeds are found to consist of straight columns with a banded structure.

Keyword: Electron beam physical vapor deposition (EB-PVD); Porosity; ZrO_2; Films

1. Introduction

Thermal barrier coatings (TBCs) of high melting point oxides on superalloy turbine parts have been used in gas turbines for some time now, leading to enhanced efficiency and performance of these devices.[1–5] A typical oxide for TBCs is partially stabilized zirconia containing 4 mol% yttria (4YSZ) because of its low density, low thermal conductivity, high melting point and good thermal shock resistance, i.e., its excellent erosion resistance properties.[6–8] Such coatings have generally been applied by plasma spraying or physical vapor deposition above a bond layer coated directly onto the turbine blade. This configuration improves the thermal efficiency of the turbine system because the low thermal conductivity of coating films allows the component to be used at higher temperatures.[9–11]

Recently, TBCs manufactured by electron beam physical vapor deposition (EB-PVD) have been favored because their unique microstructure offers the advantage of superior tolerance to mechanical strain and thermal shock at the high temperatures at which gas turbines are operated.[12–16] TBCs applied using the EB-PVD process have further advantages over the plasma spray process such as better erosion resistance, bonding strength and surface roughness of the coatings. However, the thermal conductivity of EB-PVD coatings is relatively high.

To improve the thermal performance of EB-PVD TBCs, detailed microstructural characterization of coating films is necessary because thermal properties depend strongly on microstructure. One of the advantages of using the EB-PVD technique to deposit oxide ceramics is that it is possible to vary the microstructure of the coating by controlling deposition process parameters such as coating chamber pressure, deposition rate, vapor incident angle (VIA), vapor incidence pattern (VIP) and substrate temperature. Several studies on the microstructures of YSZ films have been reported.[17–23] However, the influence of coating thickness or rotation speed on the microstructure of EB-PVD YSZ coating films has not been sufficiently explained in the literature.

The purpose of the present work is to characterize the influence of coating thickness and substrate rotation speed

* Corresponding author. Tel.: +81 52 871 3500; fax: +81 52 871 3599.
E-mail address: jang@jfcc.or.jp (B.-K. Jang).

0955-2219/$ – see front matter © 2005 Elsevier Ltd. All rights reserved.
doi:10.1016/j.jeurceramsoc.2005.03.248

on the microstructure of YSZ coatings deposited by EB-PVD on zirconia substrates.

2. Experimental procedure

Coatings were deposited by EB-PVD using commercially available 4 mol% Y_2O_3-stabilized zirconia targets. Substrates of ZrO_2–4 mol% Y_2O_3 were prepared by pressureless sintering at 1600 °C in the shape of discs of 10 mm diameter and 2 mm thickness. No bond coat between top coats and substrates was applied. Before deposition of the top coats, the substrates were ultrasonically cleaned in acetone and then isopropyl alcohol. After drying, substrates were inserted into a special holder assembly and placed into a vacuum system.

The substrates were preheated at 900–1000 °C in a preheating chamber using graphite heating elements. The substrates were then moved to the coating chamber for deposition.

The substrates were mounted on revolving holder with horizontal axis normal to the ingot. They are positioned directly above the evaporation ingot and coating surface is horizontal in rotation axis. Electron beam evaporation using a 45 kW electron gun was carried out in the coating chamber under a vacuum of 10 Pa. The target material was heated above its evaporation temperature of 3000 °C, and the resulting vapors were condensed on stationary or rotating zirconia substrates. Oxygen gas flowing at 300 cm^3/min was fed into the coating chamber during deposition to control the oxygen deficiency of the zirconia. To determine the influence of the substrate rotation speed on the microstructure of the coating layers, coated specimens were formed at different rotation speeds, namely 0 (stationary), 1, 5, 10 and 20 rpm. Total coating thicknesses in the range of 20–700 μm were obtained. The substrate temperature was 950 °C in all conditions.

X-ray diffraction (XRD) was used to determine the crystal structures of the phases present and to determine if any preferred orientation developed in the coating layers. The porosity containing nanopores in the coated layers was performed using a mercury porosimeter. The microstructures of coated specimens were observed by SEM and analyzed by energy dispersive X-ray spectroscopy (EDS). The average size of column and pore of each coating layer was obtained using the intercept method on SEM micrographs.

3. Results and discussion

3.1. Influence of coating thickness on microstructure

Typical microstructures of the upper surfaces of coatings rotated at 5 rpm for different coatings thicknesses are shown in Fig. 1. The top surfaces of the coating layers consist of square-pyramidal or cone-like grains. The microstructure of the 500 μm thick coating contains larger grains than that of the 50 μm thick coating. In addition, gaps between the

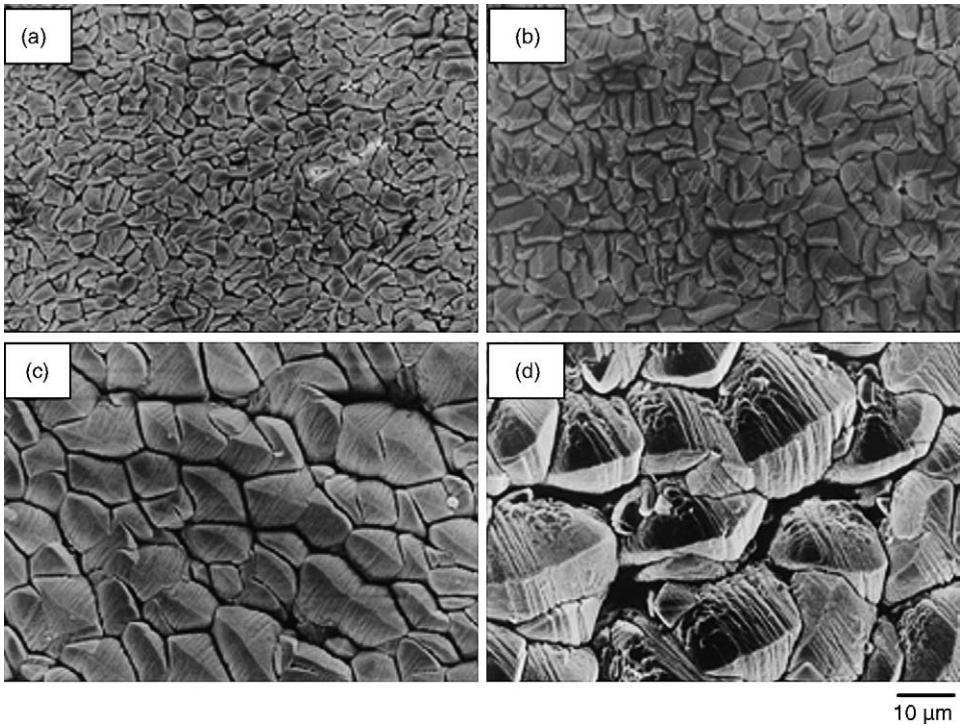

Fig. 1. SEM micrographs of surface regions of ZrO_2–4 mol% Y_2O_3 coating layers for different coating thickness obtained at 5 rpm: (a) 50 μm, (b) 100 μm, (c) 200 μm, and (d) 500 μm.

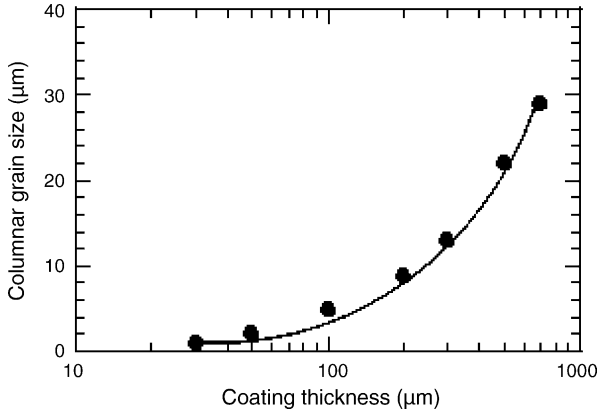

Fig. 2. Average columnar grain size of the top surface of ZrO_2–4 mol% Y_2O_3 coating layers obtained at 5 rpm as a function of coating thickness.

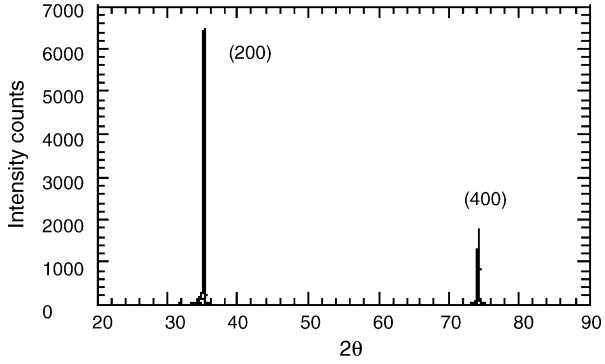

Fig. 3. XRD pattern obtained from the surface of a ZrO_2–4 mol% Y_2O_3 coating layers obtained at 5 rpm.

pyramid-like grains could be clearly observed, especially for samples with thicker coatings.

Fig. 2 shows the relationship between columnar grain size of top surface of column and coating thickness for specimens with different coating thickness. The columnar grain size increases with increasing coating thickness.

A representative XRD result at top surface of coating layers is shown in Fig. 3. This indicates that the observed phase in all present specimens is the tetragonal phase of zirconia which contain (2 0 0) and (4 0 0) reflections.

The microstructure of coating layer viewed parallel to the coating surface is shown in Fig. 4. The fracture surface of this coating layer deposited on ZrO_2 substrate clearly reveals a columnar microstructure with all the columnar grains oriented in the same direction, i.e., with their c-axes perpendicular to the substrate. Similarly textured microstructures are obtained by EB-PVD of zirconia on Inconel substrates.[1] The width of the columnar grains varies according to the distance from the substrate in spite of same crystallographic orientation of columns. Nuclei form on the substrate with random orientations at the start of deposition, and growing into grains that become better aligned as they extend upwards. At the same time, the columnar grains increase in size the thicker the coating becomes, resulting in a tapered columnar structure. Gaps between columnar grains could also be clearly observed, particularly towards the top of the coating. Such gaps were not very noticeable at the base of the columns.

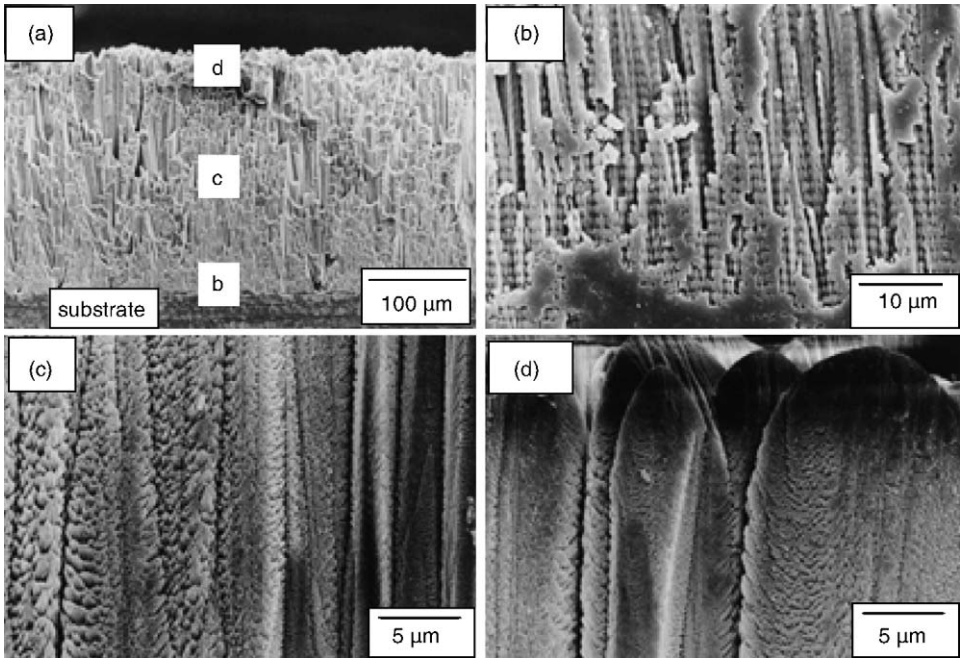

Fig. 4. SEM micrographs of (a) coating layers of 300 μm thickness obtained at 5 rpm for low magnification, and (b)–(d) magnified views at different distances from substrates of ZrO_2–4 mol% Y_2O_3 for points labeled in (a).

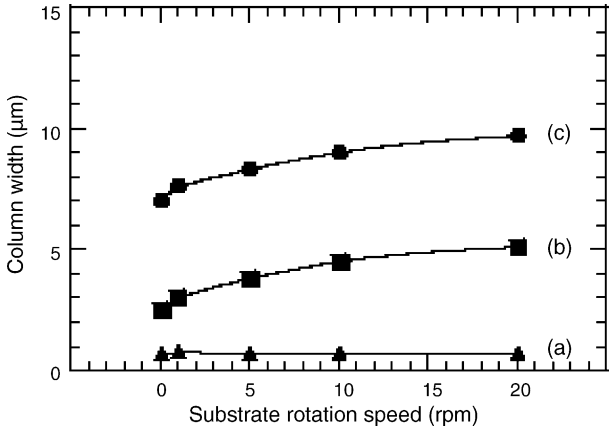

Fig. 5. Column width of measured from the sides of ZrO_2–4 mol% Y_2O_3 coating layers as a function of surface rotation speed: (a) at 5 μm from the substrate, (b) at 150 μm from the substrate, and (c) at 250 μm from the substrate.

3.2. Influence of rotation speed on microstructure

Fig. 5 shows the relationship between average column width and substrate rotation speed. The width of the columns depends strongly on the substrate rotation speed, increasing with increasing rotation speed. In addition, within the same specimen the average width of the column depends on the distance from the substrate. The widths of columns at positions further from the substrate are larger than those lower positions.

These results demonstrate that epitaxial growth of YSZ films does not occur when deposited on zirconia substrates by EB-PVD. Instead, nucleation and grain growth occur on the substrate during deposition. This is due, primarily, to coarsening and coalescence of columns as small particles nucleate on their surfaces.[21] Consequently, the coalescence of columns due to competitive columnar growth makes the columnar grains increase in size, getting thicker the further from the substrate, resulting in a tapered columnar structure.

Fig. 6 shows the morphology of the surface of a coating layer deposited at 0 rpm observed by SEM. The surfaces of deposited YSZ films have a distinct pyramid- or cone-like morphology with textured grains that are aligned perpendicular to the substrate. The surfaces of the deposited films are relatively rough because the orientation of the crystal faces of the square pyramidal tips of the columnar grains (⟨1 1 1⟩) is different to that of the growth direction (⟨1 0 0⟩). The size of the pyramidal tips strongly depends on the degree of competitive grain growth during deposition. If the substrate rotation speed is above 1 rpm, the tips of the columns at the surfaces of the coating become more cone-shaped with rounder edges, as shown in Fig. 1.

Fig. 7 shows the morphology of fracture surfaces viewed near to the substrates of coating specimens deposited at different substrate rotation speeds observed by SEM. The 0 rpm specimen in Fig. 7(a) consists of straight columns. The 1 rpm specimen was found to have a wavy or banana-type microstructure as seen in Fig. 7(b). Such banana-type growth of the columns under slow rotation at the foot area of column growth is well known phenomenon by Schulz et al.[21] They attribute that the oscillation of the substrate temperature between maximum and minimum during one

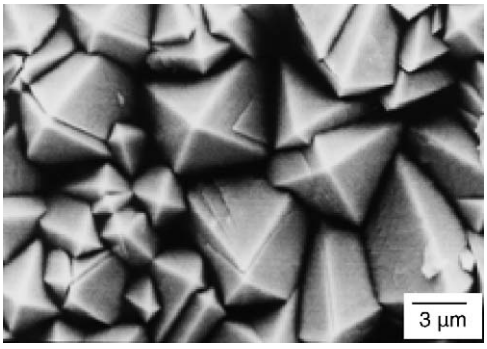

Fig. 6. SEM micrograph of the top surface of a columnar ZrO_2–4 mol% Y_2O_3 coating layers of 300 μm obtained at 0 rpm.

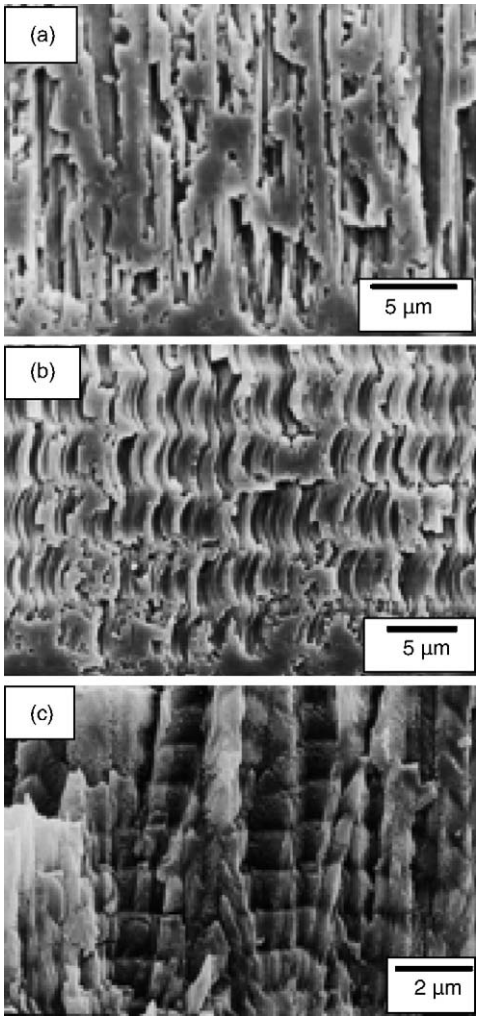

Fig. 7. SEM micrographs of columnar ZrO_2–4 mol% Y_2O_3 coating layers of 300 μm viewed near to substrate: (a) 0 rpm, (b) 1 rpm, and (c) 5 rpm.

single revolution due to radiation heating from the evaporation ingot and due to crystallization heat is responsible for the formation of the irregular column. In addition, it was reported that different zigzag-type structure with wavy or banana-type microstructure could be synthesized by alternating the position of the substrate relative to the vapor flux.[20] At higher rotation speeds, the coating did not form wavy columns. Instead, straight columns were formed with a banded structure, as seen in Fig. 7(c). Increasing the rotation speed reduces the amount of vapor particles arriving at the top of the columns and therefore the interval between each curve becomes shorter resulting in a banded structure.[21] The columnar grains in rotated specimens also had a well developed feather-like structure due to shadowing effects, with fine pores striated along the edge of the columns.

3.3. Porosity of nanoporous columns

Fig. 8 shows a plot of porosity of coating layer as a function of substrate rotation speed. The 0 rpm sample showed low porosity. Both total porosity and nano-porosity which are pores less than 50, 100 and 200 nm, respectively, increase with increasing substrate rotation speed. The nanoporous structure of coating layers results from non-equilibrium condensation of the vapor phase. The main mechanism for formation of a porous columnar structure is the so-called shadowing effect, which generally depends on the VIA or VIP of the vapor flux.[18,20–23]

In the present work, the substrate under stationary deposition conditions is always exposed to the vapor flux. Columns growth is therefore much more uniform, resulting in smoother columns which have relatively few shadowed areas, and hence low porosity. In contrast, samples deposited at higher rotation speeds have showed the increased porosity with well developed intercolumnar gaps. For specimens coated at higher rotation speeds, the vapor flow is non-uniform due to discontinuous vapor flux by revolution. The microscopic uniformity of the vapor flux at higher rotations is likely to result in more shadowed areas and hence large amounts of porosity, resulting in increased porosity with increasing rotation speed.

Fig. 9 shows SEM micrographs of nano-gaps within columns and the feather-like structure, as well as intragranular nanopores within polished YSZ columns. These pores for the rotated specimens are easily formed within shadowed areas generated by the "sunrise" and "sunset" incidence of vapor onto substrates during rotation. Two levels of shadowing can be observed in the coating microstructure, namely, intercolumnar shadowing on the micron scale, which affects the growth of the main column, as shown in Fig. 9(a), and intracolumnar shadowing on the nanometer scale, which controls the formation of the feather-like structure seen in Fig. 9(b). During deposition, the aligned "tines" of the feather-like structure separated by nano-gaps grow on both sides of the columns as shown in Fig. 9(b).

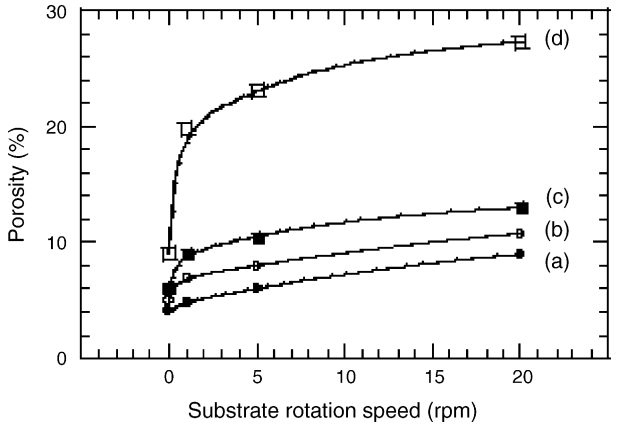

Fig. 8. Porosity of ZrO_2–4 mol% Y_2O_3 coating layers of 300 μm thickness as a function of substrate rotation speed by mercury porosimeter: (a) below 50 nm (b) below 100 nm and (c) below 200 nm of pore size and (d) total porosity.

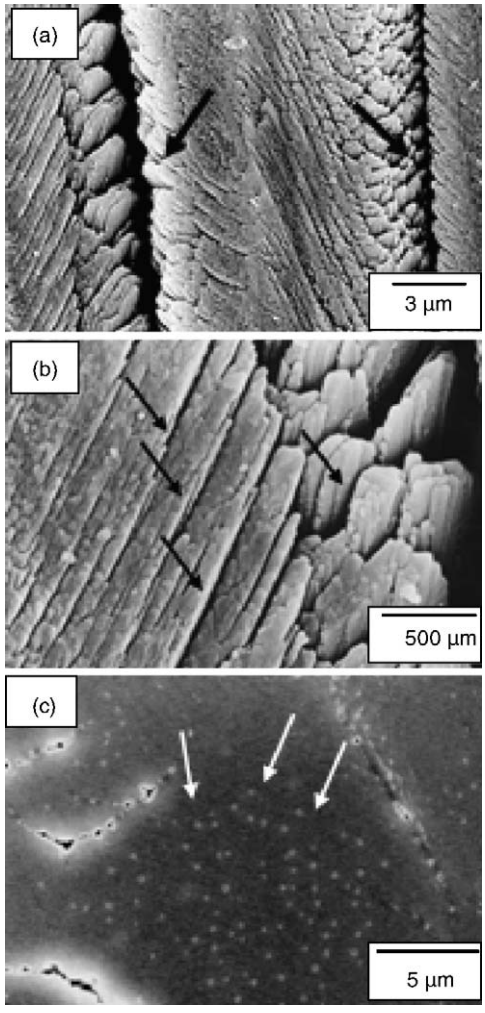

Fig. 9. SEM micrographs of nanopores of columnar ZrO_2–4 mol% Y_2O_3 coating layers of 300 μm thickness obtained at 5 rpm: (a) intercolumnar gaps between columns, (b) nano-gaps in the feather-like structure, and (c) nanopores in columnar grains.

The formation of the feather-like structure of the columns by intracolumnar shadowing can be explained as follows. The faces of the growing columns block the vapor flux, resulting in a shadowed region. However, a small number of vapor particles are able to penetrate the intercolumnar gaps and impinge on both sides of the columns at a locally oblique VIA. In addition, the intercolumnar gaps play a role in controlling the space available for vapor flux to penetrate, limiting the angular distribution of the incident flux, which leads to formation of well-aligned sub-columns on both sides of the main columns, in other words, the feather-like structure. The dendritic, feather-like structure on both sides of the columnar grains contains many micro-sized, as well as nano-sized pores. It can be concluded that the microstructure and texture of EB-PVD films are strongly influenced by shadowing of the vapor flux during deposition.[18,21] Nano-sized pores typically of diameter less than 30 nm and visible as white contrast are evident inside the columnar grains in Fig. 9(c). A high concentration of nanopores therefore exists both within the feather-like features of the columns as well as inside the columns.

4. Conclusions

Microstructural properties of ZrO_2–4 mol% Y_2O_3 coatings deposited by EB-PVD with different thicknesses and at different substrate rotation speeds on substrates of the same composition have been investigated. The coated layers had a columnar microstructure with gaps between columnar grains. The columnar grain size of the coating surfaces and the width of the columns increased with increasing coating thickness and rotation speed. The 0 rpm specimen consisted of simple, straight columns. The 1 rpm specimen had a wavy microstructure. In contrast, specimens deposited at higher rotation speeds consisted of straight columns with banded structures. The total porosity and nano-porosity of the coating layers increased with increasing substrate rotation speed. Nano-sized pores less than 50 nm in diameter could be observed inside of the columnar grains.

Acknowledgments

This work was carried out with financial support from the New Energy and Industrial Technology Development Organization (NEDO), Japan.

References

1. Levi, C. G., Emerging materials and processing for thermal barrier system. *Curr. Opin. Solid State Mater. Sci.*, 2004, **8**, 77–91.
2. Schulz, U., Saruhan, B., Fritscher, K. and Leyens, C., Review on advanced EB-PVD ceramic topcoats for TBC applications. *Int. J. Appl. Ceram. Technol.*, 2004, **1**, 302–315.
3. Ahmaniemi, S., Vippola, M., Vuoristo, P., Mäntylä, T., Cernuschi, F. and Lutterotti, L., Modified thick thermal barrier coatings: microstructural characterization. *J. Eur. Ceram. Soc.*, 2004, **24**, 2247–2258.
4. Padture, N. P., Gell, M. and Jordan, E. H., Thermal barrier coatings for gas-turbine engine applications. *Science*, 2002, **296**, 280–284.
5. Stigher, M. J., Yanar, N. M., Topping, M. G., Prttit, F. S. and Meier, G. H., Thermal barrier coatings for 21st century. *Zeit. Metal.*, 1999, **90**, 1069–1078.
6. Schulz, U., Fritscher, K., Leyens, C. and Peters, M., Influence of processing on microstructure and performance of electron beam physical vapor deposition (EB-PVD) thermal barrier coatings. *J. Eng. Gas Turbines Power*, 2002, **124**, 229–234.
7. Miller, R. A., Current status of thermal barrier coatings—an overview. *Surf. Coat. Technol.*, 1987, **1**, 10–11.
8. Xu, H. B., Gong, S. K. and Deng, L., Preparation of thermal barrier coatings for gas turbine blades by EB-PVD. *Thin Solid Films*, 1998, **334**, 98–102.
9. Yanar, N. M., Meier, G. H. and Pettit, F. S., The influence of platinum on the failure of EB-PVD YSZ TBCs on NiCoCrAlY bond coats. *Scripta Materialia*, 2002, **46**, 325–330.
10. Stecura, S., Optimization of the NiCrAl–Y/ZrO_2–Y_2O_3 thermal barrier system. NASA Report No. TM-86905. NASA, Cleveland, OH, 1985.
11. Rigney, D. V., Viguie, R., Wortman, D. J. and Skelly, D. W., PVD thermal barrier coatings applications and process development for aircraft engines. *J. Thermal Spray Technol.*, 1997, **6**, 167–175.
12. Guo, H., Xu, H., Bi, X. and Gong, S., Preparation of Al_2O_3–YSZ composite coating by EB-PVD. *Mater. Sci. Eng. A*, 2002, **325**, 389–393.
13. Guo, H., Gong, S. and Xu, H., Evaluation of hot-fatigue behaviors of EB-PVD gradient thermal barrier coatings. *Mater. Sci. Eng. A*, 2002, **325**, 261–269.
14. Terry, S. G., Jennifer, R. L. and Levi, C. G., Evolution of porosity and texture in thermal barrier coatings grown by EB-PVD. In *Elevated Temperature Coatings, Science and Technology III*, ed. J. M. Hampikian and N. B. Dahotre, The Minerals, Metals & Materials Society, 1999, pp. 13–25.
15. Nicholls, J. R., Deakin, M. J. and Rickerby, A comparison between the erosion behavior of thermal spray and electron-beam physical vapor deposition thermal barrier coatings. *Wear*, 1999, **233–235**, 352–361.
16. Singh, J., Wolfe, D. E. and Singh, J., Architecture of TBCs produced by Electron beam-physical vapor deposition (EB-PVD). *J. Mater. Sci.*, 2002, **37**, 3261–3266.
17. Gu, S., Lu, T. J., Hass, D. D. and Wadley, H. N. G., Thermal conductivity of zirconia coatings with zig-zag pore microstructures. *Acta Mater.*, 2001, **49**, 2539–2547.
18. Schulz, U., Terry, S. G. and Levi, C. G., Microstructure and texture of EB-PVD TBCs grown under different rotation modes. *Mater. Sci. Eng. A*, 2003, **360**, 319–329.
19. Zhu, D., Miller, R. A., Nagaraj, B. A. and Bruce, R. W., Thermal conductivity of EB-PVD thermal barrier coatings evaluated by a steady-state laser heat flux technique. *Surf. Coat. Technol.*, 2001, **138**, 1–8.
20. Lu, T. J., Levi, C. G., Wadley, H. N. G. and Evans, A. G., Distributed porosity as a control parameter for oxide thermal barriers made by physical vapor deposition. *J. Am. Ceram. Soc.*, 2001, **84**, 2937–2946.
21. Schulz, U., Fritscher, K., Rätzer-Scheibe, H. J., Kaysser, W. A. and Peters, M., Thermocyclic behavior of microstructurally modified EB-PVD thermal barrier coatings. *Mater. Sci. Forum*, 1997, **251**, 957–964.
22. Schulz, U., Fritscher, K. and Peters, M., EB-PVD Y_2O_3- and CeO_2/Y_2O_3-stabilized zirconia thermal barrier coatings-crystal habit and phase composition. *Surf. Coat. Technol.*, 1996, **82**, 259–269.
23. Schulz, U., Münzer, J. and Kaden, U., Influence of deposition conditions on density and microstructure of EB-PVD TBCs. *Ceram. Eng. Sci. Proc.*, 2002, **23**, 353–360.